RSC Advances

PAPER

View Article Online
View Journal | View Issue

Cite this: *RSC Adv.*, 2023, **13**, 2663

Novel N-doped carbon dots derived from citric acid and urea: fluorescent sensing for determination of metronidazole and cytotoxicity studies†

Haiyan Qi, *[ac] Lixin Qiu,[a] Xiaohong Zhang,*[a] Tonghui Yi,*[b] Jing Jing,*[d] Rokayya Sami,[e] Sitah F. Alanazi,[f] Zahrah Alqahtani,[g] Mahmood D. Aljabri*[h] and Mohammed M. Rahman[i]

Received 11th November 2022
Accepted 6th January 2023

DOI: 10.1039/d2ra07150a

rsc.li/rsc-advances

Blue emitting nitrogen-doped carbon dots were synthesized using citric acid and urea through the hydrothermal method, and the fluorescence quantum yield was 35.08%. We discovered that N-CDs featured excellent robust fluorescence stability and chemical resistance. For metronidazole detection, our N-CDs exhibited quick response time, high selectivity and sensitivity, and low cytotoxicity. Specifically, our N-CDs could detect metronidazole in the linear range of 0–179 μM, and the LOD was 0.25 μM. Furthermore, metronidazole efficaciously quenches the fluorescence of N-CDs, possibly owing to the inner filter effect. Lastly, we have employed our N-CDs to detect metronidazole in commercial metronidazole tablets with high accuracy. Overall, the newly prepared fluorescence sensor, N-CDs, demonstrated a huge potential to detect metronidazole in a simple, efficient, sensitive, and rapid manner.

1 Introduction

Metronidazole (MTZ, Fig. S1†) is an antibiotic and antiprotozoal medication to treat various infections, including bacterial vaginosis, amoebiasis and giardiasis.[1,2] It has been widely used as an antimicrobial agent in both veterinary and human medicine.[3–5] Although metronidazole has good medicinal value,[6–8] it was found to be mutagenic and listed as a possible carcinogen due to the formation of 2-hydroxymethyl metabolites in 5-nitroimidazoles metabolism. An overdose of it could cause toxic reactions and side effects, including headache, loss of appetite, blurred vision, hormonal imbalance, and seizures.[9–11] Because of its frequent use in animal husbandry and aquaculture, it has been prohibited by the European Commission and the FDA in domestic animals.[12–14] Recently, China also established a standard test for metronidazole in food.[15,16] Hence, it is necessary to build a reliable and sensitive method to detect metronidazole.

Various techniques have been utilized for metronidazole detection, including HPLC,[17,18] electrochemical sensing,[19] immunoassay[20] and spectrophotometry.[21,22] Although these analytical approaches could sense metronidazole sensitively and selectively, they require professional equipment, complicated operation, and extensive sample preparation, which hinder to detection of metronidazole in a rapid and straightforward manner.

In recent years, a new highly sensitive and selective detection method has been established by using fluorescent chemical sensors for metronidazole detection. As an impactful complement to conventional analytical techniques, carbon-dot-based optical sensors enable no need for sample preparation effort and rapid detection of various ions and molecules in a highly sensitive and selective way.[23,24] Carbon dots (CDs) is a quasi-spherical nanomaterials with a characteristic size of < 10 nm.[25] It has been widely utilized in several fields for their multiple excellent properties, including high solubility, biocompatibility, simple surface modification, anti-photobleaching, and chemical inertness.[26,27] However, due to their low fluorescence quantum yields and few active sites for modification, many efforts have been made to enhance their

[a]College of Chemistry and Chemical Engineering, Qiqihar University, Qiqihar, Heilongjiang Province, 161006, China. E-mail: qhy120@sina.com; liyunhao099@163.com

[b]Laboratory of Molecular Biology, Health Inspection Center of Qiqihar Medical University, Qiqihar 161006, Heilongjiang, China. E-mail: yitonghui@126.com

[c]Technology Innovation Center of Industrial Hemp for State Market Regulation, Qiqihar University, Qiqihar 161006, China

[d]School of Medicine and Health, Harbin Institute of Technology, No.92, West Dazhi Street, Harbin, 150000, China. E-mail: jingjing@hit.edu.cn

[e]Department of Food Science and Nutrition, College of Sciences, Taif University, P.O. 11099, Taif 21944, Saudi Arabia

[f]Imam Mohammad Ibn Saud Islamic University, College of Science, Department of Physics, Riyadh, 11642, Saudi Arabia

[g]Department of Physics, Faculty of Science, Taif University, P.O. 11099, Taif 21944, Saudi Arabia

[h]Department of Chemistry, University College in Al-Jamoum, Umm Al-Qura University, Makkah, 21955, Saudi Arabia. E-mail: mdjabri@uqu.edu.sa

[i]Department of Chemistry, Faculty of Science, King Abdulaziz University, Jeddah 21589, 80203, Saudi Arabia

† Electronic supplementary information (ESI) available. See DOI: https://doi.org/10.1039/d2ra07150a

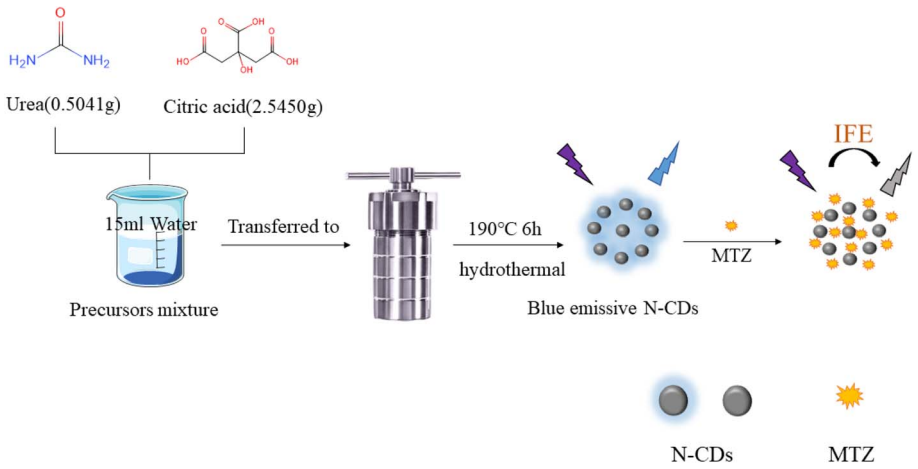

Scheme 1 Preparation of N-CDs and detection of MTZ.

luminescent properties. Doping with the non-metallic heteroatoms has been proven as a practical way to improve the fluorescence quantum yields of CDs.[28–31] Thanks to nitrogen's similar atomic size as that of carbon, and its electron donor character, the nitrogen atom becomes the natural candidate for doping in graphene and nitrogen doping has been demonstrated to improve fluorescence quantum yields with great advantages.[32–35] According to the reported papers, Humic acid, EDC-HCl, ethylenediamine, triethylenetetramine, *etc.* are usually chosen as nitrogen source in most of the carbon dots synthesis for detecting metronidazole.[36–39]

Here, in our study, citric acid and urea as starting materials were applied and prepared nitrogen-doped carbon dots (N-CDs), our nitrogen source has the following virtues: simple

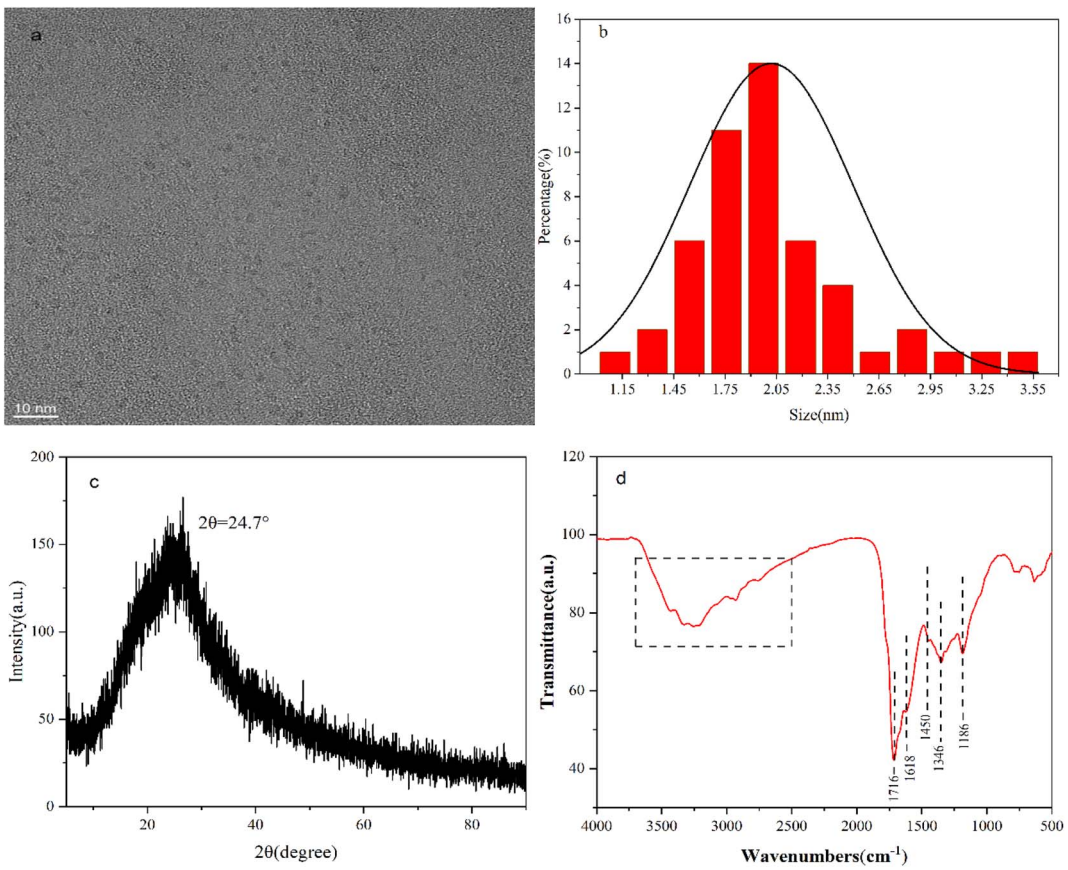

Fig. 1 (a) HRTEM image (b) particle size distribution of N-CDs (c) XRD pattern (d) FT-IR spectra.

structure, low price, safer, and easy to operate. Furthermore, our N-CDs exhibited high specificity and sensitivity to detect MTZ. Finally, our N-CDs have been successfully employed to detect metronidazole in commercial metronidazole tablets.

2 Results and discussion

2.1 N-CDs preparation and optimization

Urea and citric acid were used as the starting substances and prepared CDs by hydrothermal method (Scheme 1). To achieve high fluorescence quantum yields (QYs) of CDs, different synthetic conditions were evaluated, including reaction temperature, reactant ratio and reaction time. As expected, various reaction conditions seriously affected the QYs of CDs (Table S1–S3, and Fig. S2†). In summary, CDs were synthesized at optimized reaction conditions when the reactant ratio (urea to citric acid) at 1 : 5 and the reaction temperature at 190 °C for a total of 6 hours. The prepared CDs were named N-CDs, and the value of QY was 35.08% by the reference method.

2.2 N-CDs characterization preparation and optimization

Next, HRTEM was employed to examine the topography and particle size distributions of N-CDs. The N-CDs were dispersed and approximately spherical in shape (Fig. 1a). The particle size of N-CDs ranged from 1.04 nm to 3.42 nm, with the average size at 2.02 nm (Fig. 1b). In addition, the XRD pattern of N-CDs indicated a broad diffraction signal near 24.7°, suggesting the amorphous forms of carbon (Fig. 1c). The Raman spectrum of the N-CDs was shown in Fig. S3.† There were two prominent peaks centered at around 1350 cm^{-1} and 1581 cm^{-1}, which were ascribed to the D band (disordered band) and G band (graphite band). The ratio of I_D/I_G was 1.47. The result further confirmed that its attribution to the amorphous structure.

The N-CDs functional groups were subsequently evaluated by the FT-IR. As shown in Fig. 1d, multiple speaks were detected among 4000–500 cm^{-1}. The wide range of the peak from 3700–2500 cm^{-1} has corresponded with N–H and O–H stretching vibration. The peak at 1716 cm^{-1} was assigned to carbonyl group. The peak at 1618 cm^{-1} was ascribed to hydroxyl bending vibration. The peak at 1450 cm^{-1} was associated with the saturated C–H bending vibration. The peak at 1346 cm^{-1} was probably caused by the C–N stretching vibration, and at 1186 cm^{-1} was attributed to the C–O stretching vibration.[40,41]

To explore the detailed information about the functional groups of N-CDs and their element composition, XPS analysis was performed and observed three typical strong peaks at 531.05 eV, 399.32 eV and 284.80 eV, which were attributed to O 1s (32.00%), N 1s (9.92%) and C 1s (58.08%), respectively

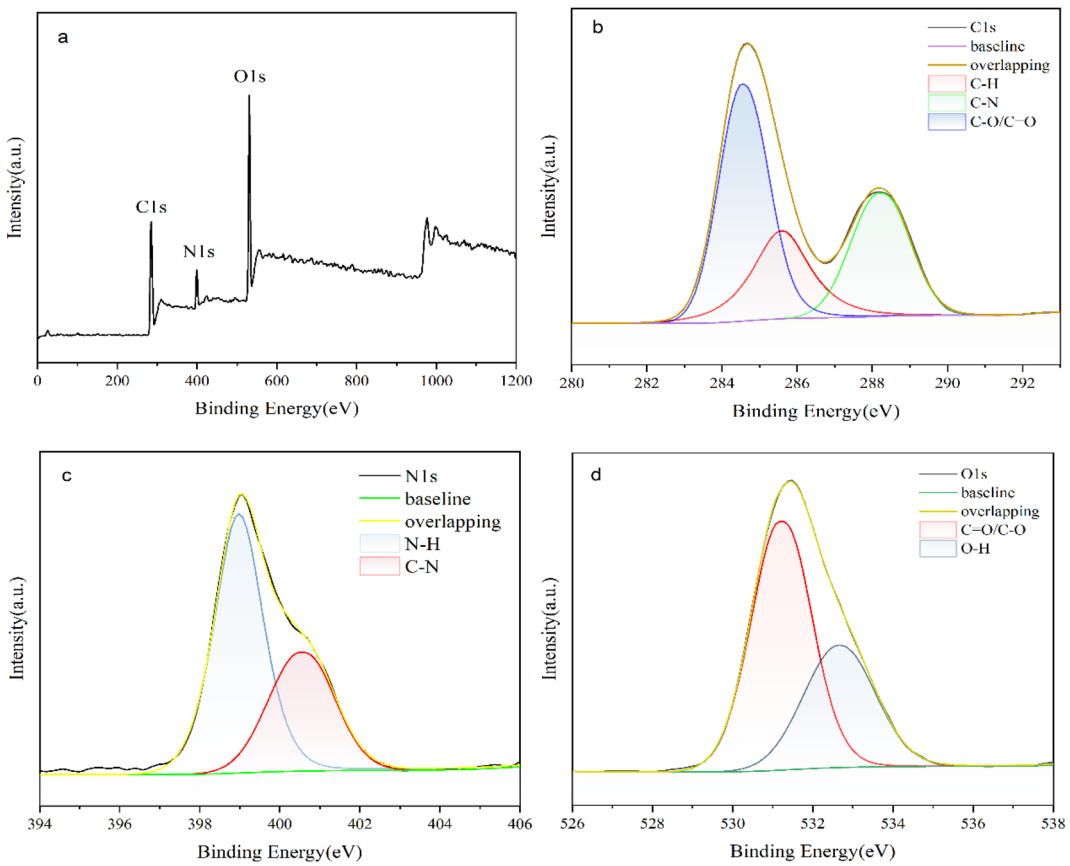

Fig. 2 (a) XPS spectrum; high-resolution XPS spectra (b) C 1s (c) N 1s (d) O 1s.

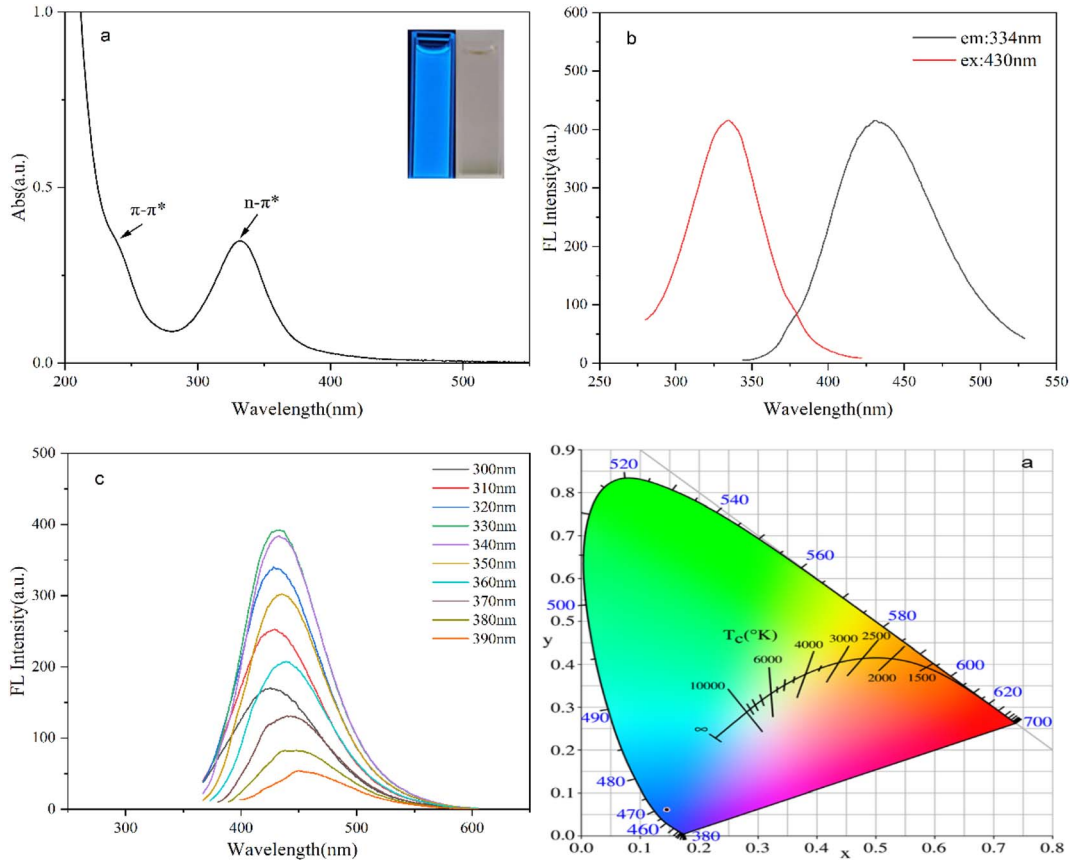

Fig. 3 (a) UV-vis spectrum (inset: under UV light (365 nm, left) and sunlight (right)) (b) fluorescence spectra of N-CDs (c) fluorescence emission spectra (d) CIE color diagram.

(Fig. 2a). Specifically, the C 1s spectra indicated three peaks at 288.18 eV, 285.58 eV and 284.54 eV, which was related to C–N, C–H and C–O/C=O bonds, respectively (Fig. 2b). The N 1s spectra displayed two decomposition peaks at 400.58 eV and 398.98 eV, which was assigned to C–N and N–H bonds (Fig. 2c). The O 1s spectra exhibited two decomposition peaks 531.17 eV and 532.65 eV, which were corresponded to O–H and C=O/C–O bonds, respectively (Fig. 2d). Lastly, the XPS data were consistent with the results obtained by FT-IR.

2.3 Optical properties of N-CDs

The Ultraviolet-visible absorption spectra of N-CDs displayed two classic absorption bands at 239 nm and 332 nm, which was

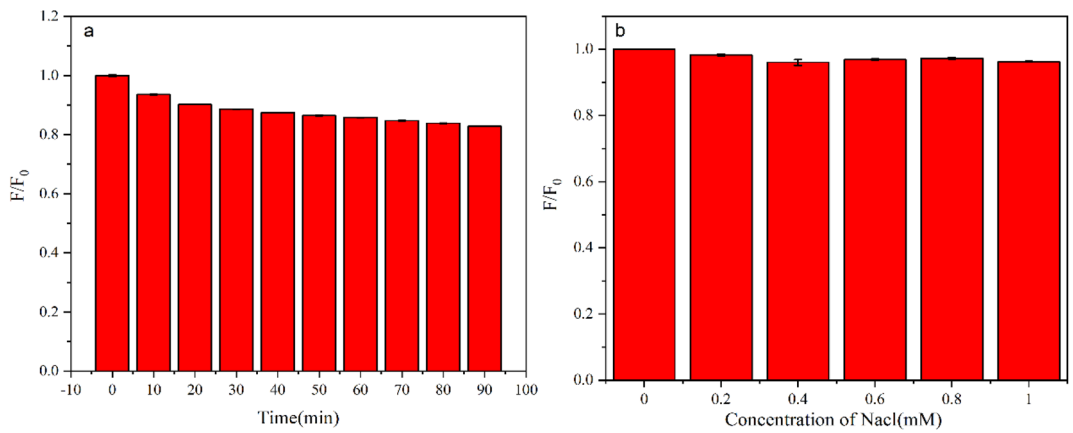

Fig. 4 (a) Effect of N-CDs photostability under continuous UV irradiation (365 nm) for various time (up to 90 min) (b) effect of ion strength (NaCl concentration of 0, 0.2, 0.4, 0.6, 0.8, 1 mM, respectively) on the photostability of N-CDs.

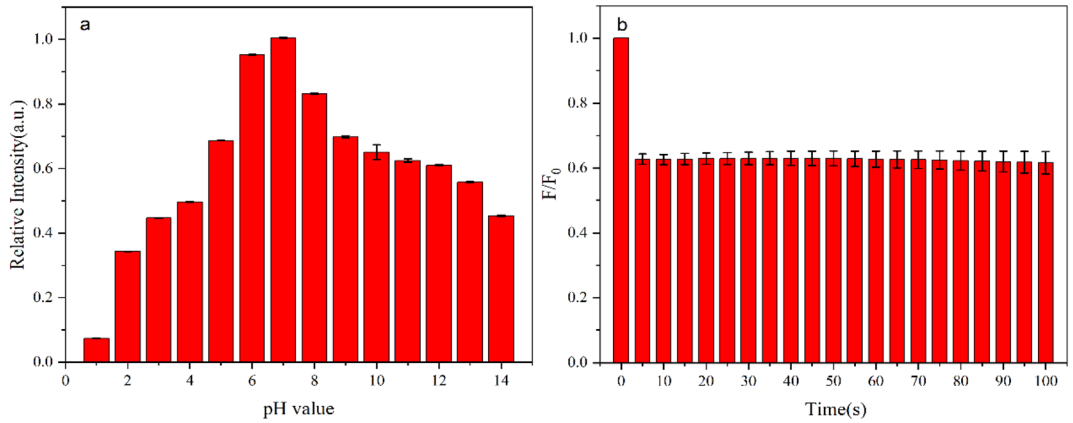

Fig. 5 (a) Effect of pH (b) the response time of N-CDs to detect metronidazole.

related to the π–π* of the carbon nucleus and the n-π* leap of C=O (Fig. 3a).[42,43] We observed the maximum wavelength of λ_{ex} and λ_{em} at 334 nm and 434 nm, respectively (Fig. 3b). Interestingly, when the excitation wavelength increased from 320 nm to 390 nm, the position of emission peak of N-CDs nearly appeared at 434 nm constantly, so it was excitation-independent (Fig. 3c). Besides, the solution of N-CDs displayed colorless and emitted blue fluorescence under sunlight and UV lamp (Fig. 3a inset). CIE color coordinate of N-CDs was calculated at (0.1515, 0.0794), further demonstrating their blue fluorescence emission with UV radiation (Fig. 3d).

Subsequently, the fluorescence stability of N-CDs was tested, illustrating its intensity with 12.53% decreased after 90 minutes ultraviolet light (365 nm) irradiation (Fig. 4a). Furthermore, the impact of salinity was explored and found the intensity of N-CDs was unaffected when the NaCl concentration reached to 1 mM (Fig. 4b), indicating their excellent chemical stability, even in extreme environmental conditions. Overall, our finding revealed that N-CDs have great potentiality in practical applications.

2.4 Detection of metronidazole

Previous studies implied pH and response time are key factors in detection, we determined to optimize them to attain better quantitative analysis of our N-CDs in metronidazole detection. The intensity of N-CDs rapidly increased in acidic environment (pH scale ranged from 1 to 7) and reached the maximum value at neutral environment (pH of 7), then gradually decreased in alkaline condition (pH scale ranged from 7 to 14) (Fig. 5a). The intensity of N-CDs still kept high (~50% of its maximum value at pH of 7) even at pH of 14, indicating that our N-CDs have high durability from weak acid to strong alkali conditions. That results might due to the influence of protonation, the fluorescence intensity of N-CDs decreases under the strong acid condition.[44,45] Next, the response time of N-CDs to metronidazole was examined. The intensity of N-CDs decreased within 5 s and remained steady and unchanged within 100 s (Fig. 5b), which suggested that the analysis time has been very short in the detection of MTZ. Therefore, pH 7 and the response time of 10 s were used for follow-up studies.

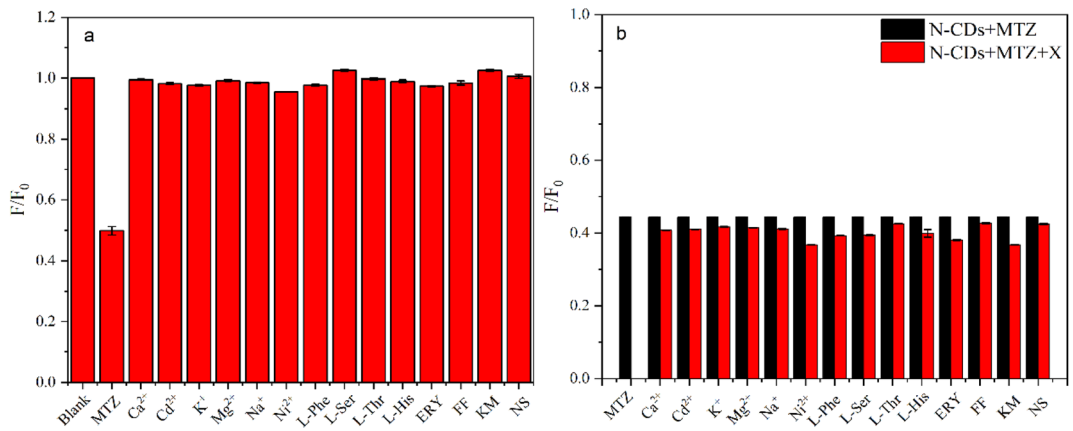

Fig. 6 (a) Effect of 400 μM various substances (MTZ, metal ions, amino acids and antibiotic) (b) effect of interference substances (when 100 μM MTZ coexisted with 500 μM metal ions, amino acids or antibiotic).

To exam the selectivity of our N-CDs to metronidazole detection, the intensity responses to other substances were measured, including various metal ions (K^+, Ca^{2+}, Mg^{2+}, Ni^{2+}, Na^+, and Cd^{2+}), four different amino acids (L-serine, L-histidine, L-threonine and L-phenylalanine) and four different antibiotics (Erythromycin, Florfenicol, Kanamycin Monsulfate, and Neomycin Sulphate). As shown in Fig. 6a, our N-CDs only responded to metronidazole, not other substances, indicating the high selectivity for metronidazole identification. Furthermore, the interference experiments by mixing metronidazole and other substances were performed. As excepted, the addition of a coexistent interference substance didn't impact the fluorescence quenching effect caused by metronidazole (Fig. 6b). Overall, the results further demonstrated that our N-CDs had high selectivity for metronidazole detection.

Next, the sensitivity of N-CDs for metronidazole detection was test. As shown in Fig. 7a, under 434 nm wavelength, with increased concentration of metronidazole (from 0 to 179 μM), the intensity of N-CDs gradually diminished. Specifically, it is apparent that the $(F_0–F)/F_0$ shown a good linear relationship to metronidazole concentration in the range of 0–24 μM, 24–87 μM and 87–179 μM (Fig. 7b). The fitted linear equations were $(F_0–F)/F_0 = 0.01361[\text{MTZ}] + 0.00628$ ($R^2 = 0.99562$), $(F_0–F)/F_0 = 0.00597[\text{MTZ}] + 0.20201$ ($R^2 = 0.99390$), and $(F_0–F)/F_0 = 0.00193[\text{MTZ}] + 0.53742$ ($R^2 = 0.99607$), respectively. The detection limit (LOD, $3\sigma/K$) was as low as 0.25 μM, indicating its sensitivity for MTZ detection. In addition, compared and summarized relevant results from previous studies, our N-CDs had wide detection range and lower LOD for metronidazole detection (Table 1).

2.5 Fluorescence quenching mechanism of MTZ detection

The Ultraviolet-visible absorption spectra of metronidazole displayed two absorption weeks at 230 nm and 322 nm (Fig. 8a). It is noticed that there was a broad overlapped band between excitation spectra of N-CDs (peaks at 334 nm) and the absorption spectra of metronidazole (Fig. 8a). Moreover, the position of the absorption peaks was unchanged, and the intensity was enhanced with the presence of metronidazole, indicating that no new complex was formed between MTZ and N-CDs and the electron–hole complex was not the cause of the burst effect (Fig. 8b).[49] To further explore the underlying mechanism, the fluorescence lifetime was examined. The fluorescence lifetime of N-CDs displays almost no change in presence of MTZ (Fig. 8c). The evidences provided that the quenching mechanism of MTZ might be due to the IFE.

2.6 Detection of MTZ in commercial samples

To examine the practicality of N-CDs for the detection of metronidazole, the metronidazole content from commercial metronidazole tablets were inspected. As described previously, the concentration of the MTZ tablet was measured as 2.10 μM, which is beyond our LOD of N-CDs. Therefore, three different concentrations of MTZ solutions (5, 10, and 15 μM) in

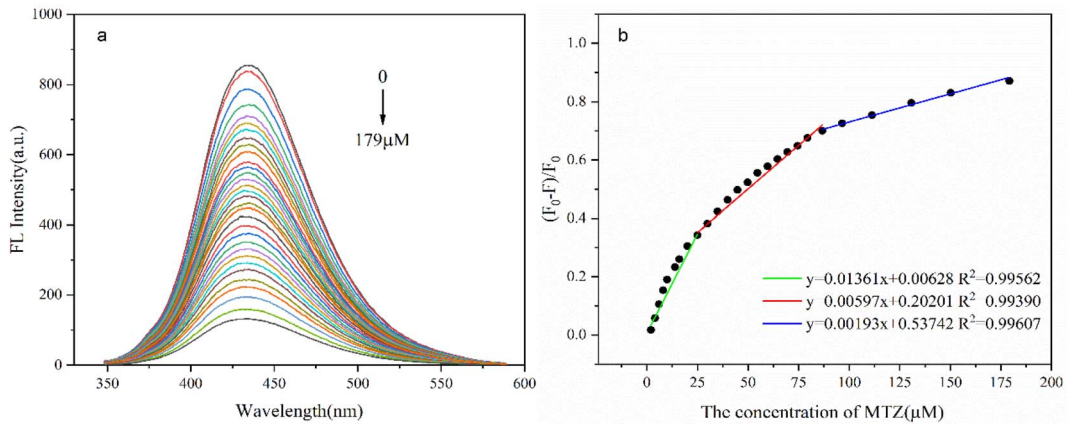

Fig. 7 (a) N-CDs response to MTZ (b) fitting curve between $(F_0–F)/F_0$ and concentration of MTZ in the range of 0–24 μM (green line), 24–87 μM (red line) and 87–179 μM (blue line).

Table 1 Comparison for MTZ detection

Sensing method or material	Linear detection range (μM)	Limit of detection (μM)	Ref.
N-CDs	5–75	0.957	37
High-performance liquid chromatography (HPLC)	0.76–1750	2.28	46
Cu-poly(cysteine)film	0.5–400	0.37	47
P-AgSA-CE	3.4–17.1	0.34	48
Carbon dots (N-CDs)	**0–179**	**0.25**	**This work**

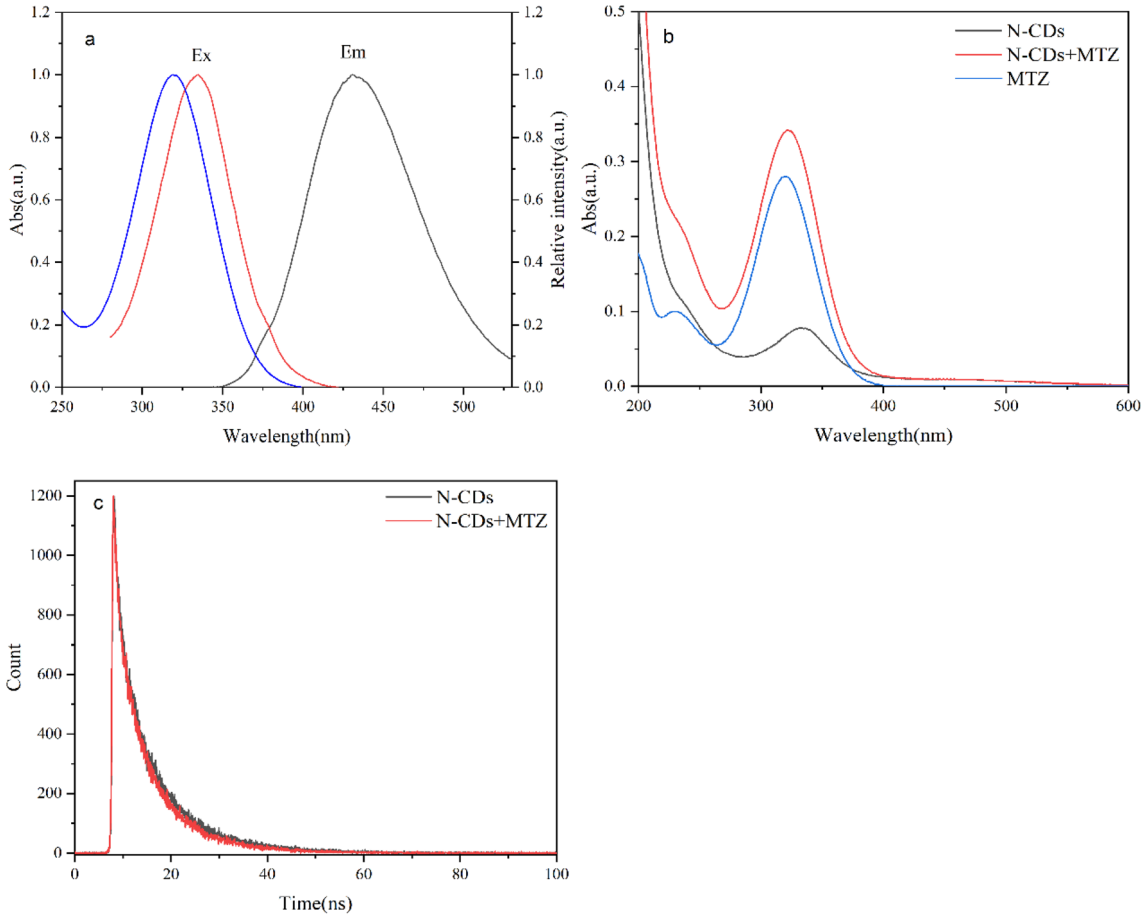

Fig. 8 (a) The excitation spectra of N-CDs and the absorbance spectra of MTZ (b) UV-vis absorbance spectra of the N-CDs (c) fluorescence decay curve of N-CDs absence and presence of MTZ.

Table 2 MTZ concentration detection in commercial tablets

Sample	MTZ in tablets (μM)	Spiked MTZ concentration (μM)	Total found (μM)	Recovery (%) $N = 3$	RSD (%) $N = 3$
MTZ tablets	2.10	5	6.80	94.00	4.70
		10	12.21	101.10	1.52
		15	16.84	98.27	4.73

commercial metronidazole tablets were spiked and evaluated the performance of our N-CDs to these mixtures. Not surprisingly, the recovery rates were calculated as high as 94.00%–101.10% (RSD < 4.73%), indicating our N-CDs had high practicability and accuracy (Table 2)

2.7 Cytotoxicity of N-CDs

Lastly, the cytotoxicity of our N-CDs in HaCaT cells with MTT assay was investigated. Increased amount of N-CDs slightly affected the HaCaT cells viability, even 100 mg mL^{-1} of N-CDs only caused 10.68% decrease of cell viability, indicating our N-CDs had low cytotoxicity (Fig. 9).

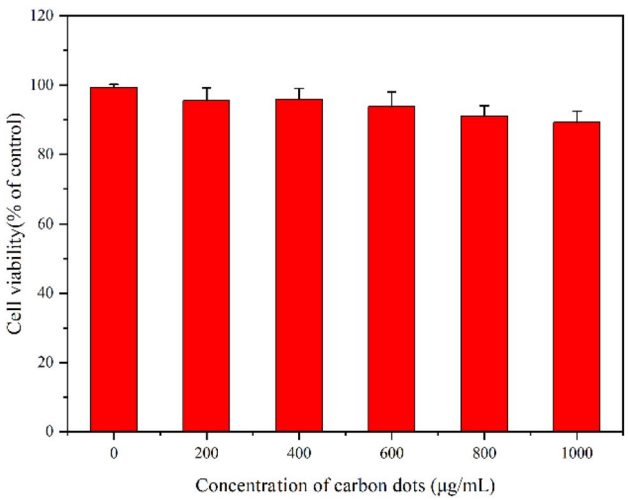

Fig. 9 MTT assay of HaCaT cells.

3 Conclusion

In summary, a new water-soluble blue-fluorescent N-doped carbon dots was synthesized, and the quantum yield was

35.08%. Our N-CDs exhibited low cytotoxicity, high specificity and sensitivity to metronidazole in a rapid manner (within 10 s). In addition, metronidazole content in commercial metronidazole tablets were successfully detected with high accuracy. Furthermore, we discovered that the IFE could be the possible quenching mechanism of MTZ detection. Above all, our N-CDs demonstrated their potential to detect metronidazole without any special instrument.

Conflicts of interest

The authors declare no competing interests.

Acknowledgements

The work is funded by the National Natural Science Foundation of China (52172092); the Fundamental Research Funds in Heilongjiang Provincial Universities (145109507, 135109207); the Deanship of Scientific Research at Umm Al-Qura University for supporting this work by Grant Code: (22UQU4290372DSR07).

References

1 G. Dahlen and H. R. Preus, *Anaerobe*, 2017, **43**, 94–98.
2 O. I. Zheltvai, Zheltvai II, V. V. Spinul and V. P. Antonovich, *J. Anal. Chem.*, 2013, **68**, 600–605.
3 Y. Liu, J. Liu, H. Tang, J. Liu, B. B. Xu, F. Yu, *et al.*, *Sens. Actuators, B*, 2015, **206**, 647–652.
4 Y. Gu, X. Y. Yan, C. Li, B. Zheng, Y. R. Li, W. L. Liu, *et al.*, *Biosens. Bioelectron.*, 2016, **77**, 393–399.
5 N. Xiao, J. Deng, J. L. Cheng, S. Q. Ju, Hq Zhao, J. Xie, *et al.*, *Biosens. Bioelectron.*, 2016, **81**, 54–60.
6 S. Benitez-Martinez, A. L. Lopez-Lorente and M. Valcarcel, *Biosens. Bioelectron.*, 2015, **121**, 6–13.
7 M. B. Gholiv and M. Torkashv, *Talanta*, 2011, **02**, 022.
8 M. E. Falagas, A. P. Grammatikos and A. Michalopoulos, *Expert Rev. Anti-Infect. Ther.*, 2008, **6**, 593–600.
9 J. Y. Han, L. Z. Zhang, S. B. Yang, J. Wang and D. H. Tan, *Bull. Environ. Contam. Toxicol.*, 2014, **92**, 196–201.
10 G. M. Tiboni, F. Marotta, A. P. Castigliego and C. Rossi, *Hum. Reprod.*, 2009, **24**, 2688–2692.
11 G. Sisson, J. Y. Jeong, A. Goodwin, L. Bryden, N. Rossler, S. Lim-Morrison, *et al.*, *J. Bacteriol.*, 2000, **182**, 18.
12 R. J. Sram, L. Dobias, P. Rossner, D. Vesela, D. Vesely, R. Rakusova, *et al.*, *Environ. Health Perspect.*, 1993, **101**, 155–158.
13 C. Q. Han, J. Chen, X. M. Wu, Y. W. Huang and Y. P. Zhao, *Talanta*, 2014, **128**, 293–298.
14 J. R. Zhao, X. H. Pan, X. B. Sun, W. Pan, G. F. Yu and J. P. Wang, *Luminescence*, 2018, **33**, 704–712.
15 W. Liu, J. Zhang, C. Li, L. Tang, Z. Zhang and M. Yang, *Talanta*, 2013, **104**, 204–211.
16 D. Chen, J. Deng, J. Liang, J. Xie, C. H. Hu and K. H. Huang, *Sens. Actuators, B*, 2013, **183**, 594–600.
17 H. M. Maher, R. M. Youssef, R. H. Khalil and S. M. El-Bahr, *J. Chromatogr. B: Anal. Technol. Biomed. Life Sci.*, 2008, **876**, 175–181.
18 T. Parusu and V. Ponneri, *Eur. J. Chem.*, 2009, **2**, 865–868.
19 Y. Nikodimos and M. Amare, *J. Anal. Methods Chem.*, 2016, **2016**, 3612943.
20 C. S. Thompson, I. M. Traynor, T. L. Fodey and S. R. H. Crooks, *Anal. Chim. Acta*, 2009, **637**, 259–264.
21 M. A. Korany, H. H. Abdine, M. A. A. Ragab and S. I. Aboras, *Spectrochim. Acta, Part A*, 2015, **143**, 281–287.
22 O. I. Zheltvai, Zheltvai II and J. Spinul VV, *J. Anal. Chem.*, 2013, **68**, 600–605.
23 Y. H. Liu, W. X. Duan, W. Song, J. J. Liu, C. Ren, *et al.*, *ACS Appl. Mater. Interfaces*, 2017, **9**, 12663–12672.
24 H. Y. Qi, Q. Y. Li, J. Jing, T. Jing, C. T. Liu, L. X. Qiu, *et al.*, *Nanomaterials*, 2022, **12**, 976.
25 L. Dordevic, F. Arcudi, M. Cacioppo and M. Prato, *Nat. Nanotechnol.*, 2022, **17**, 112–130.
26 H. Q. Tao, K. Yang, Z. Ma, J. M. Wan, Y. J. Zhang, Z. H. Kang, *et al.*, *Small*, 2012, **8**, 281–290.
27 Y. L. Wang, P. Anilkumar, L. Cao, J. H. Liu, P. J. G. Luo, K. N. Tackett, *et al.*, *Exp. Biol. Med.*, 2011, **236**, 1231–1238.
28 Y. S. Ma, Y. Cen, M. Sohil, G. H. Xu, F. D. Wei, M. L. Shi, *et al.*, *ACS Appl. Mater. Interfaces*, 2017, **9**, 33011–33019.
29 Y. Q. Zhang, X. Y. Liu, Y. Fan, X. Y. Guo, L. Zhou, Y. Lv, *et al.*, *Nanoscale*, 2016, **8**, 15281–15287.
30 C. L. Tan, C. Zhou, X. Y. Peng, H. Z. Zhi, D. Wang, Q. Q. Zhan, *et al.*, *Nanoscale Res. Lett.*, 2018, **13**, 272.
31 J. C. Ge, Q. Y. Jia, W. M. Liu, L. Guo, Q. Y. Liu, M. H. Lan, *et al.*, *Adv. Mater.*, 2015, **27**, 4169–4177.
32 X. Hai, J. Feng, X. W. Chen and J. H. Wang, *J. Mater. Chem. B*, 2018, **6**, 3219–3234.
33 Q. Hu, L. Gao, S. Q. Rao, Z. Q. Yang, T. Li and X. J. Gong, *Food Chem.*, 2019, **280**, 195–202.
34 Y. Liu, X. J. Gong, W. J. Dong, R. X. Zhou, S. M. Shuang and C. Dong, *Talanta*, 2018, **183**, 61–69.
35 H. F. Wu and C. L. Tong, *J. Agric. Food Chem.*, 2019, **67**, 2794–2800.
36 Z. G. He, J. X. Liu, C. Zhang, Y. D. Sun, Q. Chen, J. Zhang, *et al.*, *Anal. Bioanal. Chem.*, 2022, DOI: **10.1007/s00216-022-04291-1**.
37 J. Y. Du, C. F. Wang, P. C. Yuan, Q. Shu, N. Xu, Y. Yang, *et al.*, *Anal. Methods*, 2021, **13**, 4652–4661.
38 X. X. Wang, T. Lin, W. Wu, H. S. Wu and D. D. Yan, *Environ. Technol.*, 2021, **43**, 4213–4226.
39 G. D. Ren, X. Y. Hou, Y. Kang, R. Zhang, M. Zhang, W. Liu, *et al.*, *Spectrochim. Acta, Part A*, 2020, **234**.
40 M. S. Masoud, A. A. Ibrahim and E. A. Khalil, *Spectrochim. Acta, Part A*, 2007, **67**, 662–668.
41 S. Sarkar, S. Dutta, C. Ray, B. Dutta, J. Chowdhury and T. Pal, *CrystEngComm*, 2015, **17**, 8119–8129.
42 S. Sarkar, J. Chowdhury, S. Dutta and T. Pal, *Spectrochim. Acta, Part A*, 2016, **169**, 109–115.
43 C. J. Reckmeier, J. Schneider, Y. Xiong, J. Hausler, P. Kasak, W. Schnick, *et al.*, *Chem. Mater.*, 2017, **29**, 10352–10361.

44 Q. Wang, H. Y. Zhang, D. M. Yu, W. Qin and X. H. Wu, *Carbon*, 2022, **198**, 162–170.
45 J. Yang, X. L. Jin, Z. Cheng, H. W. Zhou, L. N. Gao, D. L. Jiang, *et al.*, *ACS Sustainable Chem. Eng.*, 2021, **9**, 13206–13214.
46 N. Tavakoli, J. Varshosaz, F. Dorkoosh and M. R. Zargarzadeh, *J. Pharm. Biomed. Anal.*, 2007, **43**, 325–329.
47 Y. Gu, X. Y. Yan, W. L. Liu, C. Li, R. X. Chen, L. Tang, *et al.*, *Electrochim. Acta*, 2015, **152**, 108–116.
48 V. Vyskocil, T. Navratil, A. Danhel, J. Dedik, Z. Krejcova, L. Skvorova, *et al.*, *Electroanal*, 2011, **23**, 129–139.
49 Y. L. Liu, Q. X. Zhou, Y. Y. Yuan and Y. L. Wu, *Carbon*, 2017, **115**, 550–560.